


 CrossMark
click for updates

 Cite this: *CrystEngComm*, 2015, 17, 8555

Cationic surfactant-assisted hydrothermal synthesis: an effective way to tune the crystalline phase and morphology of SAPO molecular sieves†

 Miao Yang,^a Peng Tian,^a Lin Liu,^a Chan Wang,^{ab} Shutao Xu,^a Yanli He^a and Zhongmin Liu^{*a}

The present work investigates the effect of cationic surfactants on tuning the crystalline phase and morphology of SAPO molecular sieves. First, we explore the cationic surfactant-assisted hydrothermal synthesis of DNL-6, which is a newly developed SAPO molecular sieve with RHO structure and can be prepared only in a narrow silica concentration. Comparative experiments reveal that the cationic surfactant with a longer alkane chain can help to obtain pure DNL-6 with an adjustable Si content, and the product with a higher Si content presents a spherical morphology composed of DNL-6 nanocrystals. It is believed that the strong adsorption of the cationic surfactant molecules on the SAPO species protects the DNL-6 from dissolving and inhibits the crystallization of SAPO-34. It is thus concluded that the cationic surfactant favors the formation of SAPO crystals having a relatively high structural symmetry although the surfactants are not retained in the product. Moreover, the crystal morphology may be modified due to the abundant interactions of the cationic surfactant with the anionic SAPO framework. Based on the above understanding, flower-like SAPO-35 and Si-rich SAPO-16 were further synthesized by designed cationic surfactant-assisted syntheses. These confirm that the cationic surfactant-assisted hydrothermal synthesis has huge potential in the control of the SAPO crystalline phase and crystal morphology. More importantly, the obtained hierarchical porous DNL-6 exhibits high catalytic activity and selectivity for the cycloaddition of CO₂ with epichlorohydrin without any solvent and co-catalyst.

 Received 24th August 2015,
Accepted 2nd October 2015

DOI: 10.1039/c5ce01702e

www.rsc.org/crystengcomm

Introduction

Aluminophosphate (AlPO) molecular sieves and their derivatives, with abundant open-framework structures, are one of the important branches of the zeolite family.^{1,2} When the framework atoms of AlPO₄ are isomorphously substituted by Si, silicoaluminophosphate (SAPO) molecular sieves with good thermal/hydrothermal stability and acidity are obtained, which thus have many significant applications in the fields of catalysis and adsorption/separation.^{3–5} A large number of experiments and theoretical calculations have been implemented to establish the relationship between the crystal structure, morphology and properties of SAPO molecular sieves.^{6–12} But, few efforts have been made directly towards the synthesis of a new SAPO phase although it may create the

possibility to establish a new industrial process with high efficiency.^{13,14} The rational synthesis of SAPO molecular sieves with targeted structures and functions remains a formidable task due to the limited understanding on the crystallization of SAPO systems and the inefficient trial-and-error exploration. Recently, a series of work concerning the crystallization mechanism of open-framework aluminophosphates and the structure-directing effect in the crystallization of such materials have been reported.^{15–19} The investigations demonstrate once again that the crystallization of inorganic microporous materials is a very complicated process. Even though the structure-directing effect of a template is the most important key for the formation of an open-framework structure, there are still many other factors that can change the reaction results, such as the solvent or the other additives.

Small-pore molecular sieves with a large cavity structure have unique advantages for gas adsorption/separation and selective catalysis because of their critical aperture size around 4 Å and high micropore volume.²⁰ In 2011, our laboratory reported a new small pore SAPO molecular sieve, DNL-6, with RHO topology.¹⁴ It crystallizes in the cubic system, has the *I*23 space group, and is built up by *α*-cavities connected through double 8-rings. The material can

^a Dalian National Laboratory for Clean Energy, National Engineering Laboratory for Methanol to Olefins, Dalian Institute of Chemical Physics, Chinese Academy of Sciences, Dalian, PR China. E-mail: liuzm@dicp.ac.cn

^b University of Chinese Academy of Sciences, Beijing, PR China

† Electronic supplementary information (ESI) available: Synthesis and characterization details of nanosized DNL-6, SAPO-35, SAPO-16 and SAPO-44. ¹H and ¹³C NMR data of the products obtained from the catalytic reactions. See DOI: 10.1039/c5ce01702e

accommodate high concentrations of single $\text{Si}(\text{OAl})_4$ species which exhibits huge potential in $\text{CO}_2/\text{N}_2(\text{CH}_4)$ adsorption/separation.⁵ At first, DNL-6 was found accidentally during the investigation of the phase-transformation process of SAPO molecular sieves.¹⁴ After that, several new synthetic strategies including cationic surfactant-assistant hydrothermal synthesis,²¹ aminothermal synthesis²² and dry-gel conversion⁵ have been developed to prepare DNL-6. Notably, each synthetic method has a very narrow crystallization region, and the Si content of the DNL-6 product cannot be adjusted continuously by any method. Although the hydrothermal synthesis method is the most popular one to prepare SAPO molecular sieves, DNL-6 has never been detected previously possibly due to the critical requirements for the silica and alumina sources. Moreover, the cationic surfactant cetyltrimethylammonium bromide (C_{16}TAB) seems to be indispensable even though diethylamine (DEA) is the only guest molecule in DNL-6. It is also puzzling that the Si content of the reactant gel has to be precisely controlled, otherwise, the product will be contaminated with SAPO-34. It is very important to understand the role of the cationic surfactant and the crystallization process of DNL-6, which may help to guide the synthesis of SAPO molecular sieves.

In this work, DNL-6 was hydrothermally synthesized without and with a series of alkyltrimethyl ammonium bromides containing C12, C16 and C18 alkyl chains, respectively. The DNL-6 seed was added if necessary. The role of a cationic surfactant was investigated and discussed in detail based on the experimental results accompanied with the series of expanded experiments. An effective way to tune the Si content of DNL-6 has been found. Moreover, DNL-6s with enriched hierarchical porosity and nano size have also been hydrothermally synthesized during this study which exhibit high catalytic activity and selectivity for the cycloaddition reaction of carbon dioxide with epichlorohydrin without any solvent and co-catalyst. This work provides inspiration towards the design and synthesis of new SAPO molecular sieve materials.

Experimental section

Materials

All the reactants, orthophosphoric acid (H_3PO_4 , 85 wt%), tetraethyl orthosilicate (TEOS), aluminium isopropoxide ($\text{Al}(\text{i-C}_3\text{H}_7\text{O})_3$), diethylamine (DEA), hexamethyleneimine (HMI), dodecyltrimethyl ammonium bromide (C_{12}TAB , $\text{C}_{12}\text{H}_{25}(\text{CH}_3)_3\text{NBr}$), hexadecyltrimethyl ammonium bromide (C_{16}TAB , $\text{C}_{16}\text{H}_{33}(\text{CH}_3)_3\text{NBr}$) and octadecyltrimethyl ammonium bromide (C_{18}TAB , $\text{C}_{18}\text{H}_{37}(\text{CH}_3)_3\text{NBr}$) were used as received without further purification.

Synthesis

The typical hydrothermal synthesis procedure of the SAPO molecular sieves is as follows. Desired amounts of $\text{Al}(\text{i-C}_3\text{H}_7\text{O})_3$, H_3PO_4 , TEOS and organic amine (DEA or HMI) were added into deionized water in sequence. If necessary, a

quantitative amount of a cationic surfactant or a DNL-6 seed was subsequently added. Stirring was maintained during all the mixing procedures above. The final gel mixture was transferred into a stainless-steel autoclave and heated up to 200 °C under rotation. After a certain reaction time, the autoclave was cooled down by cold water, and the solid product was washed thoroughly with distilled water, recovered by centrifugation and dried at 110 °C overnight. If necessary, the samples were calcined at 600 °C for 5 h to remove the template.

Characterization

The powder XRD patterns were recorded on a PANalytical X'Pert PRO X-ray diffractometer, with $\text{Cu-K}\alpha$ radiation ($\lambda = 1.54059 \text{ \AA}$), operating at 40 kV and 40 mA. The chemical compositions of the samples were determined using a Philips Magix-601 X-ray fluorescence (XRF) spectrometer. The crystal morphology was observed by scanning electron microscopy (SEM, Hitachi TM3000 and SU8020). The selected area electron diffraction (SAED) patterns were recorded using a JEM-2100 electron microscope. Textural properties of the calcined samples were determined by N_2 adsorption at 77 K using a Micromeritics Gemini VII 2390 surface area analyzer. The total surface area was calculated based on the BET equation. The micropore volume and micropore surface area were evaluated by using the t -plot method. The mesopore volume and mesopore surface area were evaluated from the adsorption isotherm by the Barrett–Joyner–Halenda (BJH) method. The wettability of the selected material was examined using a Drop Shape Analysis System, DSA100, Krüss on the surface of a pressed pellet. The contact angles were measured using the image of a sessile drop at the points of intersection (three-phase contact points) between the drop contour and the projection of the surface (baseline). The zeta potential of the selected sample was determined by using a Malvern Zetasizer Nano ZS90. The measurement was performed on a solution where less than 1 mg of the sample was dispersed in 5 g of distilled water with ultrasonic treatments for over 3 min.

Catalyst evaluation

The synthesized DNL-6s were used directly as catalysts to synthesize chloropropene carbonate through cycloaddition of CO_2 with epichlorohydrin. In a typical reaction, 2.0 ml of epichlorohydrin and 0.2 g of catalyst were loaded into a 100 mL high pressure stainless steel Parr reactor. The reactor was pressurized with CO_2 at 12 bar, and the reaction was carried out at 120 °C for 4 h. After the reaction, the reactor was cooled to room temperature, and the unreacted CO_2 was vented out. The catalyst was separated by centrifugation. The products were identified by ^1H and ^{13}C NMR spectroscopy (Varian 7600 AS400 MHz) and GC-MS (HP7890 gas chromatograph equipped with a HP-5 column). The temperature ramp rate during the GC analysis is as follows: 25 °C min^{-1} from 80 to 250 °C.

Results and discussion

Synthesis and characterization of DNL-6

The crystallization of DNL-6 is a result of concerted actions of manifold factors. Herein, we focus on varying the alkyl chain length of the cationic surfactant and the silica amount of the starting gel. The reaction conditions are kept at 200 °C for 24 h. As seen in Table 1 and Fig. S1,[†] the final product is a combination of DNL-6 and SAPO-34 when C₁₂TAB is used. Highly crystallized DNL-6 can be prepared in the presence of C₁₆TAB or C₁₈TAB. It is worth noting that C₁₈TAB is a powerful barrier to prevent the formation of SAPO-34. By using C₁₈TAB, DNL-6 is the sole SAPO product (sample 9) even if the Si/Al ratio is up to 0.8. Comparatively, a minor amount of SAPO-34 will appear when C₁₆TAB is used and the Si/Al ratio reaches 0.6 (sample 5). It is also interesting to find that the morphology of DNL-6 changes obviously with the increase in the Si/Al ratio. As seen in Fig. 1, sample 6 exists as rhombic polyhedral single crystals with smooth crystal faces, while the crystal edges of sample 7 become unclear as the Si/Al ratio increases. The morphology of sample 8 becomes sphere-like and the crystal surface is quite rough. Sample 8 is actually an aggregation of countless DNL-6 nanocrystals, as seen in the high resolution SEM in Fig. 1, in the left corner. Notably, the selected area electron diffraction (SAED) pattern (inset in Fig. 1) gives highly discrete diffraction spots indicating the single crystal feature of sample 8. Although sample 9 is still spherical, its XRD intensity is very weak indicating a low crystallinity and the presence of an amorphous phase. The N₂ adsorption/desorption experiment was used to evaluate the texture properties of sample 8, and the adsorption isotherm is shown in the right corner in Fig. 1. It gives a typical Type I isotherm and has a large N₂ uptake near $P/P_0 = 0$ due to the microporous adsorption. The inclination and the visible hysteresis loop in the $0.7 < P/P_0 < 0.9$ region are attributed to the multilayer adsorption between the intercrystal pores of the nanoparticles. The BET surface area and the micropore

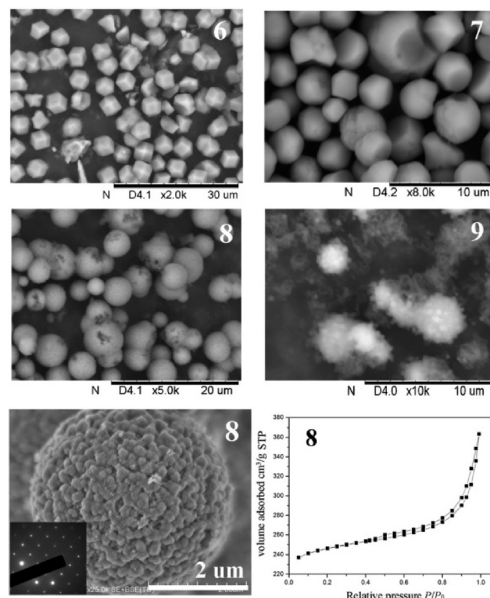


Fig. 1 SEM images of samples 6–9, and the N₂ adsorption–desorption isotherm of sample 8 (right corner). The inset is a SAED pattern of sample 8.

volume of 747 m² g⁻¹ and 0.33 cm³ g⁻¹, respectively, are comparable to those of the conventional DNL-6 (ref. 21) indicating a high crystallinity (Table S1[†]). The large external surface area of 106 m² g⁻¹ and the mesopore volume of 0.15 cm³ g⁻¹ confirm the existence of mesopores caused by the aggregation of the nanocrystals. Interestingly, some DNL-6 products have been observed to be hydrophobic during the sample washing which are further confirmed through the Drop Shape Analysis System. As illustrated in Fig. 2, the water contact angle of sample 8 is 144.4° belonging to a hydrophobic region. In contrast, the calcined sample 8 displays complete wetting properties and the droplet will be adsorbed instantaneously upon touching the sample pellet. It is thus believed that the hydrophobic surface properties of the as-synthesized sample 8 are related to the surface adsorption of the surfactants. The sample will become hydrophilic again upon the removal of the adsorbed surfactants.

Role of the cationic surfactants

The adsorption behavior of a cationic surfactant gives us a clue to understand its role in the hydrothermal synthesis.

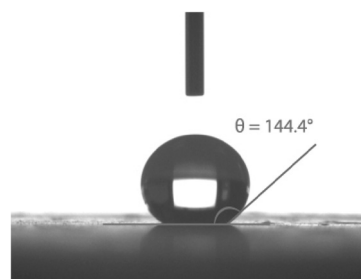


Fig. 2 A sessile water droplet on sample 8.

Table 1 Synthetic conditions and results with different cationic surfactants^a

Samples	Cationic surfactants	x /TEOS	Products	Si/Al/P compositions
1	C ₁₂ TAB	0.2	DNL-6 & SAPO-34	N/A
2	C ₁₂ TAB	0.4	DNL-6 & SAPO-34	N/A
3	C ₁₆ TAB	0.2	DNL-6	0.115/0.516/0.369
4	C ₁₆ TAB	0.4	DNL-6	0.194/0.470/0.336
5	C ₁₆ TAB	0.6	DNL-6 & SAPO-34	N/A
6	C ₁₈ TAB	0.2	DNL-6	0.121/0.514/0.365
7	C ₁₈ TAB	0.4	DNL-6	0.183/0.518/0.298
8	C ₁₈ TAB	0.6	DNL-6	0.263/0.442/0.295
9	C ₁₈ TAB	0.8	DNL-6	0.332/0.404/0.265

^a The initial gel molar composition is 0.8 H₃PO₄ : 1.0 Al(i-C₃H₇O)₃ : x TEOS : 1.5 DEA : 50 H₂O : 0.2 cationic surfactant, $x = 0.2$ – 0.8 , crystallization conditions: 200 °C, 24 h.

Three sets of parallel comparative experiments with the initial gel molar composition of 0.8 H_3PO_4 : 1.0 $\text{Al}(\text{i-C}_3\text{H}_7\text{O})_3$: 0.2 TEOS : 1.5 DEA : 50 H_2O : 0 surfactant or 0.3 C_{12}TAB or 0.2 C_{18}TAB have been further conducted keeping different reaction times. The experimental results are exhibited in Fig. 3. As seen in Fig. 3a, even if the surfactant is absent, DNL-6 with a uniform spherical morphology still crystallizes in the initial stage of the reaction (1.2 h). It indicates that the nucleation of DNL-6 is quite fast, and the surfactant is not necessary for the nucleation. At 1.5 h, a SAPO-34 impurity can be detected by the XRD, which turns into a main product at 2.0 h. Along with the reaction, the liquid environment changes which prefers the formation of SAPO-34. DNL-6 can be seen as a metastable phase for the crystallization of SAPO-34. A crystalline layered AlPO_4F intermediate had been identified during the synthesis of SAPO-34 in the presence of HF and morpholine as a structure-directing agent.²³ In our case, the formation of the DNL-6 intermediate may be due to the usage of the special reactant combination of TEOS, $\text{Al}(\text{i-C}_3\text{H}_7\text{O})_3$ and DEA. It should be mentioned that once $\text{Al}(\text{i-C}_3\text{H}_7\text{O})_3$ is replaced with pseudoboehmite, DNL-6 cannot be crystallized under the current conditions. The Al source, with different chemical and physical properties, may lead to a different local concentration of free aluminum species which results in a different crystallization behavior.^{24,25} The phase transformation from DNL-6 to SAPO-34 can be modified by adding a cationic surfactant. As seen in Fig. 3b, when C_{12}TAB is introduced without changing any other conditions, the product at 2.0 h is DNL-6 with very low

crystallinity. The crystallinity gets much better after another two hours (4.0 h), and the polyhedral morphology of the product forms which is over 10 μm . Notably, if the reaction lasts for another two hours, the DNL-6 product is contaminated with some SAPO-34 impurities reflecting in the XRD pattern. The crystal size of DNL-6 shrinks and the crystallinity gets worse which suggest a possible crystal dissolution process. If C_{18}TAB is used instead of C_{12}TAB , DNL-6 is always the product, and the crystal size of DNL-6 keeps increasing (Fig. 3c). Based on the above results, it is believed that the initially crystallized DNL-6 is not stable. The DNL-6 tends to dissolve in the mother liquid where SAPO-34 is consequently crystallized. If the cationic surfactants are introduced, the dissolution of DNL-6 and the crystallization of SAPO-34 are both inhibited. According to the surfactant adsorption theory, the surfactants with longer hydrocarbon chains have a much greater driving force for aggregation.^{26,27} It is thus believed that the interactions of C_{12}TAB with the negatively charged SAPO species are weaker than those of C_{16}TAB and C_{18}TAB so that DNL-6 embryos cannot be stabilized well when C_{12}TAB is used. As a result, DNL-6 crystals with SAPO-34 impurity crystallize finally. C_{18}TAB can provide the most powerful support for the crystallization of DNL-6 and its further growth. It is believed that the strong electrostatic interactions of the cationic surfactants with the anionic SAPO species offer them a relatively hydrophobic and safe environment with highly symmetric charge distribution. As a result, DNL-6 with a cubic structural symmetry stays stable, and the crystallization of SAPO-34 with a trigonal or a hexagonal system is inhibited.

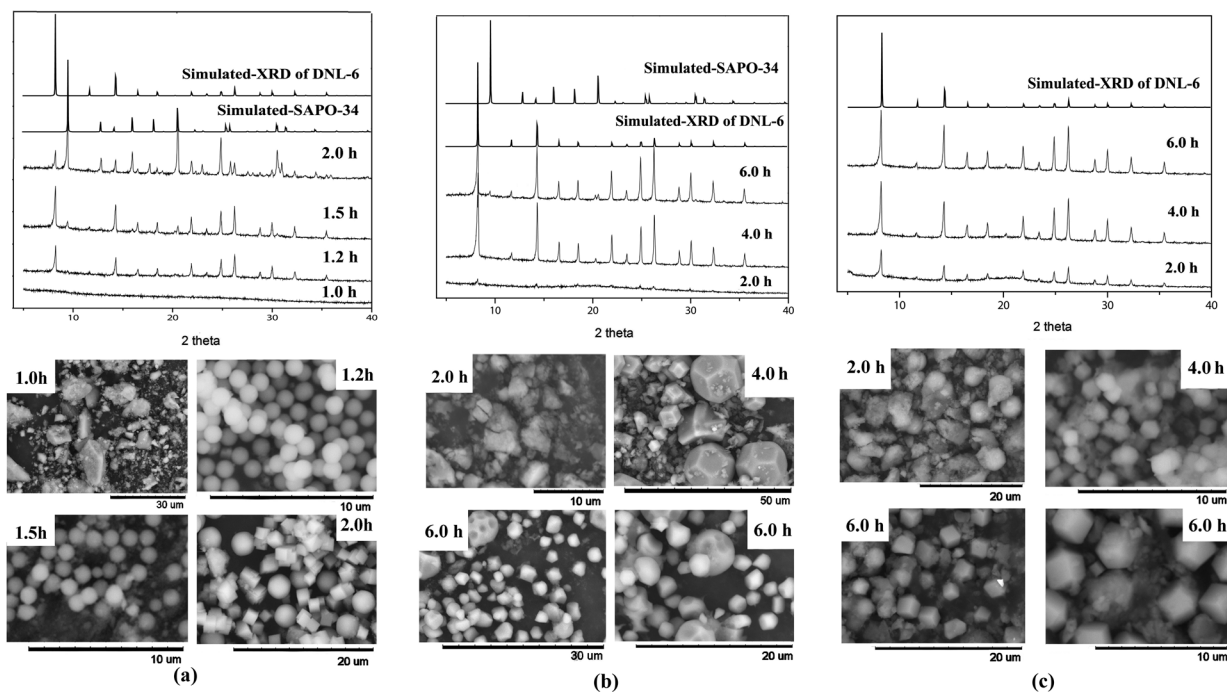


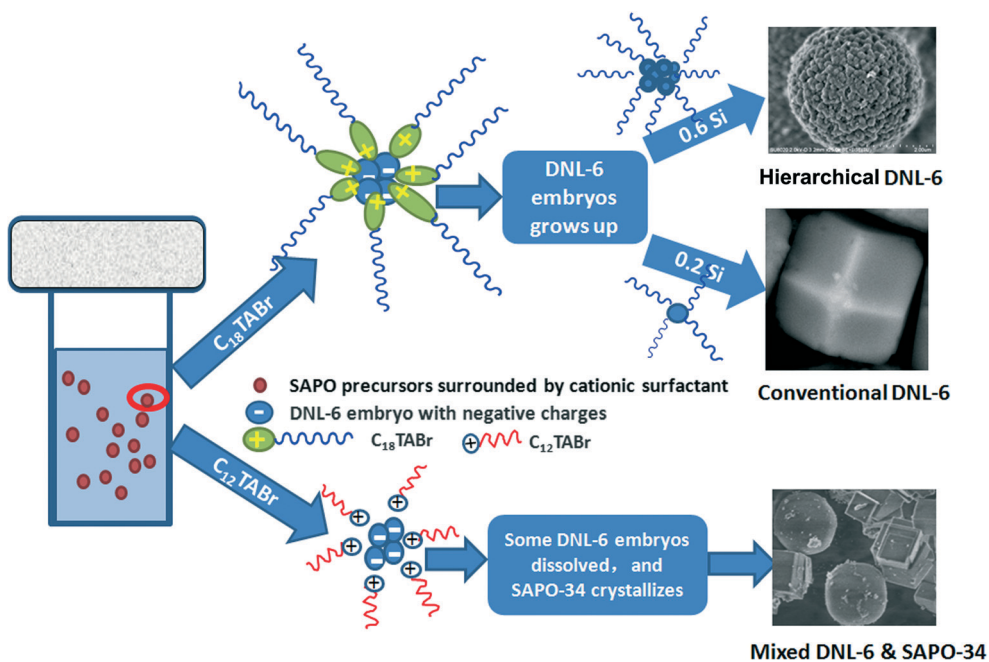
Fig. 3 XRD patterns (above) and SEM images (below) of SAPO molecular sieves crystallized at different reaction times, (a) without any surfactant, (b) with C_{12}TAB , and (c) with C_{18}TAB .

The zeta potential is the potential difference between the dispersion medium and the stationary layer of fluid attached to the dispersed particle, which is widely used for quantification of the magnitude of the charge. In order to know the nature of the initially crystallized DNL-6 precursor, the spherical DNL-6 product obtained in the reaction subjected for 1.2 hours without using any surfactant (Fig. 3a, 1.2 h) was selected to measure the zeta potential. It gave a negative potential of -36.0 eV. The result confirms the possibility for the electrostatic interactions between the initially formed DNL-6 crystals and the cationic surfactants. A similar negatively charged SAPO-11 precursor has also been reported by Bao, *et al.*²⁸ Although the embryo of DNL-6 is not stable, the adsorbed cationic surfactant molecules on the DNL-6 crystal surface protect them from dissolving and keep them growing up. Besides the effect on the SAPO phase selectivity, the adsorbed cationic surfactant can also change the crystal morphology. The negative charges of the SAPO precursor come from the introduction of Si atoms into the neutral AlPO_4 framework. So, a Si-rich precursor may load more negative charges and thus adsorbs more cationic surfactant molecules. The crystal growth is therefore severely disturbed which results in the spherical products composed of DNL-6 nanocrystals. Inversely, the crystal presents a normal morphology when the adsorbed surfactants are not enough.

A hydrothermal crystallization process for the DNL-6 molecular sieve is proposed based on the above analysis and is illustrated in Scheme 1. Negatively charged DNL-6 embryos are firstly formed. The cationic surfactants adsorb on the precursor surface due to the electrostatic interactions offering the embryos a symmetric charge distribution environment

suitable for the crystallization of DNL-6. If the doped silica amount is large and the precursor has more negative charges, there will be more surfactant molecules adsorbed on the surface of the precursor. The growth of the DNL-6 precursor thus receives more interference which leads to a spherical aggregation of DNL-6 nanoparticles. When the number of adsorbed cationic surfactants is low for the Si-poor DNL-6 embryos, the DNL-6 crystal morphology remains normal. If the cationic surfactant is absent or the interactions between the cationic surfactants and the embryos decrease, the assistant structure-directing role of the cationic surfactant would become weak. Consequently, some DNL-6 crystals will dissolve in the mother liquid, and the environment changes preferring the crystallization of SAPO-34. The two phases might reach a balance in a certain proportion depending on the reaction conditions.

The above investigation clearly shows that the cationic surfactant has significant impacts on the phase selectivity and morphology of the SAPO molecular sieves. The cationic surfactant protects DNL-6 from dissolving and thus inhibits the crystallization of SAPO-34, which can be seen as a sort of additive favoring the growth of DNL-6 crystals. If so, can DNL-6 seeds replace the cationic surfactant molecules to support the crystallization of DNL-6? A milled DNL-6 seed was introduced instead of the cationic surfactant to synthesize DNL-6 in our further investigation. Nano-DNL-6 with a particle size of *ca.* 150 nm has been obtained at 200 °C for 24 h, as shown in Fig. 4. Notably, the nanosized DNL-6 can be used continuously to synthesize pure DNL-6 in nanoscale, named Nano-DNL-6-R. Comparatively, using the as-synthesized micrometer-size DNL-6s as seeds can only achieve a mixture of DNL-6 and SAPO-34, and the particle size is close to 1 μm .



Scheme 1 Effects of cationic surfactants on the crystallization of DNL-6 molecular sieves.

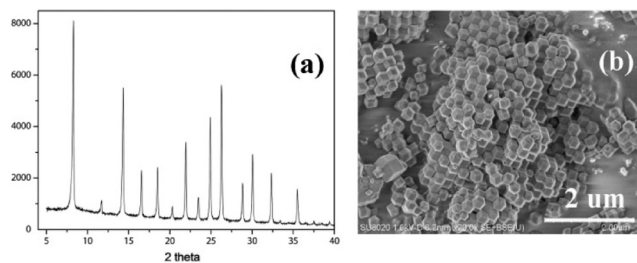


Fig. 4 XRD pattern (a) and SEM image (b) of nanosized DNL-6.

The synthesis and characterization details are presented in the ESI including Table S1 and Fig. S2.† These results confirm again that the cationic surfactant is not necessary for the nucleation of DNL-6. The milled DNL-6 precursor provides the crystallization system enough DNL-6 nuclei. As a result, the crystallization of DNL-6 is promoted, and the formation of SAPO-34 is avoided. For the first time, we achieve a Si-rich nanosized DNL-6 under hydrothermal conditions without any surfactant.

Expanded synthesis

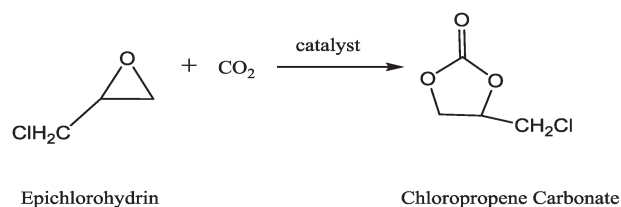
The understanding of the role of the cationic surfactants prompted us to synthesize more SAPO molecular sieves with another organic amine template. Hexamethylenimine (HMI) was used to synthesize SAPO molecular sieves with the assistance of C_{18} TAB. Flower-like SAPO-35 was achieved due to the presence of C_{18} TAB. More interestingly, Si-rich SAPO-16 with an AST topology was also obtained when the silica source is further increased. Conventionally, SAPO-44 would be the final product with the increase in the silica amount in the absence of the surfactant. Herein, the crystallization of the new SAPO-16 product is due to the contribution of C_{18} TAB. For more synthesis and characterization details, see the ESI including Table S2, Fig. S3 and S4.† Similar to SAPO-34, SAPO-44 also has a CHA topology structure with a trigonal symmetry, while the structural symmetry of SAPO-16 belongs to the cubic system. This phase selectivity process agrees with our above speculation. The presence of a cationic surfactant facilitates the crystallization of SAPO molecular sieves having a relatively high structural symmetry. So, the product changes to SAPO-16 instead of SAPO-44. To the best of our knowledge, this is the first report on the synthesis of SAPO-35 with a flower-like morphology which may provide this small-pore SAPO molecular sieve a possible application in catalysis. In addition, SAPO-16 was previously synthesized only by large templates of quinuclidine or bis(cyclopentadienyl) cobalt(III) hydroxide, and the Si content of the product is quite low (2.7–3.6 wt%).²⁹ Herein, SAPO-16 is directed by the HMI template with the assistance of C_{18} TAB, and the Si content is significantly increased to 10.2%. The synthesis of flower-like SAPO-35 and Si-rich SAPO-16 demonstrates once again the role of a cationic surfactant on the phase selectivity and morphology during the SAPO molecular sieve crystallization

which provides a huge space for the exploration of the new material.

Catalytic property evaluation

We recently reported on the excellent CO_2/N_2 adsorption/separation ability of DNL-6,⁵ which may favor the catalytic conversion of CO_2 to cyclic carbonates. The CO_2 cycloaddition reaction presents an appealing approach to effectively use the greenhouse gas CO_2 to produce chemical compounds.³⁰ Moreover, cyclic carbonates are very useful chemical intermediates, electrolyte components in lithium batteries and polar solvents. Up to now, most cyclic carbonates are manufactured with the highly toxic phosgene as a catalyst. Although an alternative non-phosgene route based on the quaternary ammonium salt-based catalysts has been developed by BASF and Chimei-Asahi Corporation (Taiwan),³¹ the reaction has to be carried out at high temperature (180–200 °C)/pressure (50–80 bar) for high yields. In some cases, a solvent was essential for high selectivity. Recently, some porous materials including zeolites,³² mesoporous materials,^{33,34} and zeolite imidazolate frameworks (ZIFs)³⁵ have been reported to be active for this kind of reaction. But the investigation on the catalytic performance of silicoaluminophosphates is quite rare.³⁶

In this work, the as-synthesized DNL-6s were used to catalyze the cycloaddition reaction of CO_2 with epichlorohydrin (Scheme 2) directly. The catalytic results are summarized in Table 2. All the DNL-6s are active for this reaction. The reaction conditions are mild, and no solvent or co-catalyst is required. Notably, the hierarchical porous (sample 8) and nanosized (Nano-DNL-6-R) DNL-6 crystals exhibit higher conversion and selectivity which may be attributed to their larger external surface areas. Further investigation on the catalytic reaction is still underway.



Scheme 2 Cycloaddition reaction of CO_2 with epichlorohydrin.

Table 2 Catalytic performance of SAPO molecular sieves in the cycloaddition reaction of CO_2 with epichlorohydrin^a

Catalysts	Epichlorohydrin conversion (%)	Yield of chloropropene carbonate (%)
Sample 6	80.6	65.7
Sample 7	73.8	73.3
Sample 8	95.4	88.4
Nano-DNL-6-R	99.3	86.6

^a Reaction conditions: epichlorohydrin, 2 mL; catalyst, 20 mg; CO_2 pressure, 12 bar; temperature, 120 °C; time, 4 h.

Conclusions

In summary, the role of a cationic surfactant in the hydrothermal synthesis of SAPO molecular sieves was investigated well by taking a DNL-6 synthetic system as the model. The electrostatic interactions of the cationic surfactants with the negatively charged SAPO species cover the DNL-6 embryos to grow up gradually, which inhibit the formation of the SAPO-34 molecular sieve simultaneously. The morphology modification on the DNL-6 product is realized meanwhile due to the interference of the surfactants adsorbed on the crystal surface. A Si-rich hierarchical porous DNL-6 with high activity and selectivity for the CO₂ cycloaddition reaction has thus been achieved for the first time. The role of a cationic surfactant in the phase selectivity and morphology control is further proven to be applicable for other SAPO molecular sieve syntheses. SAPO-35 with a flower-like morphology and Si-rich SAPO-16 have also been hydrothermally synthesized for the first time with the assistance of a cationic surfactant. More SAPO molecular sieves with new structures and morphologies are expected to be prepared through this cationic surfactant-assisted hydrothermal synthesis strategy.

Acknowledgements

We thank Dr. Haibo Xie for giving the (chloromethyl)ethylene carbonate standard sample. We are grateful for the financial support from the National Natural Science Foundation of China (NSFC no. 21476228 and 21101150).

References

- S. T. Wilson, B. M. Lok, C. A. Messina, T. R. Cannan and E. M. Flanigen, *J. Am. Chem. Soc.*, 1982, **104**, 1146.
- B. M. Lok, C. A. Messina, R. L. Patton, R. T. Gajek, T. R. Cannan and E. M. Flanigen, *J. Am. Chem. Soc.*, 1984, **106**, 6092.
- J. H. Yu and R. R. Xu, *Chem. Soc. Rev.*, 2006, **35**, 593.
- Z. D. Zhu, M. Hartmann and L. Kevan, *Chem. Mater.*, 2000, **12**, 2781.
- X. Su, P. Tian, D. Fan, Q. Xia, Y. Yang, S. Xu, L. Zhang, Y. Zhang, D. Wang and Z. Liu, *ChemSusChem*, 2013, **6**, 911.
- D. Barthomeuf, *Zeolites*, 1994, **14**, 394.
- G. Sastre, D. W. Lewis and C. R. A. Catlow, *J. Phys. Chem. B*, 1997, **101**, 5249.
- D. Chen, K. Moljord, T. Fuglerud and A. Holmen, *Microporous Mesoporous Mater.*, 1999, **29**, 191.
- I. M. Dahl, R. Wendelbo, A. Andersen, D. Akporiaye, H. Mostad and T. Fuglerud, *Microporous Mesoporous Mater.*, 1999, **29**, 159.
- F. C. Sena, B. F. de Souza, N. C. de Almeida, J. S. Cardoso and L. D. Fernandes, *Appl. Catal., A*, 2011, **406**, 59.
- G. Yang, Y. Wei, S. Xu, J. Chen, J. Li, Z. Li, J. Yu and R. Xu, *J. Phys. Chem. C*, 2013, **117**, 8214.
- X. Su, S. Xu, P. Tian, J. Li, A. Zheng, Q. Wang, M. Yang, Y. Wei, F. Deng and Z. Liu, *J. Phys. Chem. C*, 2015, **119**, 2589.
- M. Afeworki, G. J. Kennedy, D. L. Dorset and K. G. Strohmaier, *Chem. Mater.*, 2006, **18**, 1705.
- P. Tian, X. Su, Y. Wang, Q. Xia, Y. Zhang, D. Fan, S. Meng and Z. Liu, *Chem. Mater.*, 2011, **23**, 1406.
- W. Yan, X. Song and R. Xu, *Microporous Mesoporous Mater.*, 2009, **123**, 50.
- B. Zhang, J. Xu, F. Fan, Q. Guo, X. Tong, W. Yan, J. Yu, F. Deng, C. Li and R. Xu, *Microporous Mesoporous Mater.*, 2012, **147**, 212.
- X. Tong, J. Xu, C. Wang, H. Lu, P. Huang, W. Yan, J. Yu, F. Deng and R. Xu, *Microporous Mesoporous Mater.*, 2012, **155**, 153.
- X. Tong, J. Xu, L. Xin, P. Huang, H. Lu, C. Wang, W. Yan, J. Yu, F. Deng, H. Sun and R. Xu, *Microporous Mesoporous Mater.*, 2012, **164**, 56.
- P. Huang, J. Xu, C. Wang, F. Deng and W. Yan, *RSC Adv.*, 2014, **4**, 39011.
- M. Moliner, C. Martinez and A. Corma, *Chem. Mater.*, 2014, **26**, 246.
- X. Su, P. Tian, J. Li, Y. Zhang, S. Meng, Y. He, D. Fan and Z. Liu, *Microporous Mesoporous Mater.*, 2011, **144**, 113.
- D. Fan, P. Tian, S. Xu, Q. Xia, X. Su, L. Zhang, Y. Zhang, Y. He and Z. Liu, *J. Mater. Chem.*, 2012, **22**, 6568.
- O. B. Vistad, D. E. Akporiaye and K. P. Lillerud, *J. Phys. Chem. B*, 2001, **105**, 12437.
- X. Tong, J. Xu, C. Wang, W. Yan, J. Yu, F. Deng and R. Xu, *Microporous Mesoporous Mater.*, 2014, **183**, 108.
- H. Lu, J. Xu, P. Gao, W. Yan, F. Deng and R. Xu, *Microporous Mesoporous Mater.*, 2015, **208**, 105.
- R. Atkin, V. S. J. Craig, E. J. Wanless and S. Biggs, *Adv. Colloid Interface Sci.*, 2003, **103**, 219.
- S. Paria and K. C. Khilar, *Adv. Colloid Interface Sci.*, 2004, **110**, 75.
- L. Guo, X. Bao, Y. Fan, G. Shi, H. Liu and D. Bai, *J. Catal.*, 2012, **294**, 161.
- K. J. Balkus Jr., A. G. Gabrielov and N. Sandler, *J. Porous Mater.*, 1995, **1**, 199.
- M. Zhu and M. A. Carreon, *J. Appl. Polym. Sci.*, 2014, **131**, 39738.
- S. Fukuoka, M. Kawamura, K. Komiyama, M. Tojo, H. Hachiya, K. Hasegawa, M. Aminaka, H. Okamoto, I. Fukawa and S. Konno, *Green Chem.*, 2003, **5**, 497.
- R. Srivastava, D. Srinivas and P. Ratnasamy, *Appl. Catal., A*, 2005, **289**, 128.
- R. Srivastava, D. Srinivas and P. Ratnasamy, *Tetrahedron Lett.*, 2006, **47**, 4213.
- R. Srivastava, D. Srinivas and P. Ratnasamy, *J. Catal.*, 2005, **233**, 1.
- C. M. Miralda, E. E. Macias, M. Zhu, P. Ratnasamy and M. A. Carreon, *ACS Catal.*, 2012, **2**, 180.
- Z. Xie, M. Zhu, A. Nambo, J. B. Jasinski and M. A. Carreon, *Dalton Trans.*, 2013, **42**, 6732.